Regimes of wave type patterning driven by refractory actin feedback: transition from static polarization to dynamic wave behaviour

2012 Phys. Biol. 9 046005

(http://iopscience.iop.org/1478-3975/9/4/046005)

Phys. Biol. **9** (2012) 046005 (11pp) doi:10.1088/1478-3975/9/4/046005

Regimes of wave type patterning driven by refractory actin feedback: transition from static polarization to dynamic wave behaviour

W R Holmes[1], **A E Carlsson**[2] **and L Edelstein-Keshet**[1]

[1] Department of Mathematics, The University of British Columbia, Vancouver, BC V6T 1Z2, Canada
[2] Department of Physics, Washington University, St. Louis, MO 63130, USA

E-mail: wrholmes@math.ubc.ca

Received 13 April 2012
Accepted for publication 14 June 2012
Published 11 July 2012
Online at stacks.iop.org/PhysBio/9/046005

Abstract
Patterns of waves, patches, and peaks of actin are observed experimentally in many living cells. Models of this phenomenon have been based on the interplay between filamentous actin (F-actin) and its nucleation promoting factors (NPFs) that activate the Arp2/3 complex. Here we present an alternative biologically-motivated model for F-actin-NPF interaction based on properties of GTPases acting as NPFs. GTPases (such as Cdc42, Rac) are known to promote actin nucleation, and to have active membrane-bound and inactive cytosolic forms. The model is a natural extension of a previous mathematical mini-model of small GTPases that generates static cell polarization. Like other modellers, we assume that F-actin negative feedback shapes the observed patterns by suppressing the trailing edge of NPF-generated wave-fronts, hence localizing the activity spatially. We find that our NPF-actin model generates a rich set of behaviours, spanning a transition from static polarization to single pulses, reflecting waves, wave trains, and oscillations localized at the cell edge. The model is developed with simplicity in mind to investigate the interaction between nucleation promoting factor kinetics and negative feedback. It explains distinct types of pattern initiation mechanisms, and identifies parameter regimes corresponding to distinct behaviours. We show that weak actin feedback yields static patterning, moderate feedback yields dynamical behaviour such as travelling waves, and strong feedback can lead to wave trains or total suppression of patterning. We use a recently introduced nonlinear bifurcation analysis to explore the parameter space of this model and predict its behaviour with simulations validating those results.

1. Introduction

The nucleation and growth of the actin cytoskeleton is highly regulated in eukaryotic cells. Signalling networks and their downstream effectors control the nucleation, polymerization, severing, and depolymerization of filamentous actin (F-actin). Among such signalling agents are small GTPases, with Cdc42 and Rac universally recognized to be central regulators of the cytoskeleton that shape F-actin dynamics[1–4]. Complex interactions between regulatory networks and F-actin give rise to spontaneous spatio-temporal patterns such as moving spots and spatially localized waves, observed in *Dictyostelium* [5, 6], neutrophils [7], fibroblasts [8], and other cell types. Recent studies using total internal reflection microscopy (TIRF) and improved fluorescent labels [9–12] have implicated nucleation promoting factors (NPFs) such as Hem1 and WASP in their formation. Whether F-actin waves have a functional significance is unclear, but it has been speculated that they are related to the cell's exploration of its environment [7, 13], phagocytosis [14] and/or edge protrusion [15]. While the term NPF usually refers to proteins such as (WASP) and Scar/Wave, here we apply this terminology in a slightly nonstandard way,

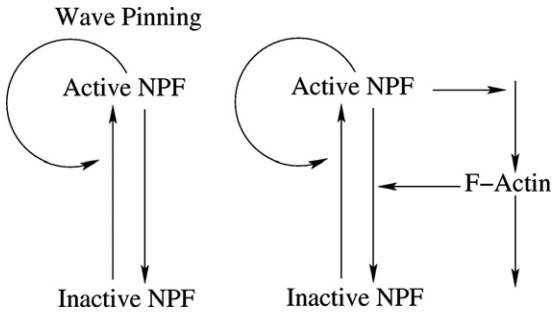

Figure 1. Schematic diagrams of models discussed in this paper. Left: the pure nucleation promotion factor (NPF) system is based on the wave-pinning model of Mori *et al* [25]. Right: NPF/refractory actin system with a constant pool of actin monomers (not explicitly modelled).

to small GTPases that are upstream of these proteins, and that hence, also promote actin polymerization.

This paper is aimed at elucidating the roles of nucleation promoting factor activation and F-actin negative feedback (weak versus strong) in the development of dynamic patterns. We are motivated by two related biophysical systems. (1) Small GTPases (such as Cdc42, Rac) are known to promote actin growth and are good candidates for NPF's [3]. At the same time, a variety of experimental observations have provided evidence for feedback from F-actin to upstream signalling complexes, whether via the Phosphoinositide 3-kinase (PI3K) pathway [16–18] which links phosphoinositide crosstalk with small GTPases [19, 20], or by reciprocal interactions of cytoskeletal proteins with integrins and the resultant signalling events (see [21, 22] for a review). Previous theoretical models [23–25], reviewed in [26], consider polarization as a standing wave of biochemical activity. In one such GTPase model, denoted 'wave-pinning (WP)' [25, 27], a sufficiently large stimulus produces a travelling wave that stalls, leaving a polarized state. We investigate how embedding this GTPase module in a circuit that includes F-actin feedback leads to dynamic wave-like patterns. (2) Our second motivation is to contribute to previous theoretical analyses of actin waves [7, 28–32], reviewed in [33] by slightly changing the focus away from detailed, more complex treatment of actin. Most previous actin-waves models include either length or angular distributions of actin or even model individual filaments [30]. We remove this complexity and instead systematically probe the effects of the interactions between NPF's and F-actin. The resulting model is analytically tractable and displays rich dynamic behaviour, including static polarization, single waves that traverse the domain, persistent reflecting waves, wave trains, and oscillations localized at the cell edge. Our model suggests that nucleation promoting factor/filamentous actin (NPF/F-actin) interactions alone are capable of producing rich dynamic patterning.

2. Model discussion

In the models discussed below, the actin nucleation promoting factor has two forms, an active membrane bound form (A), and an inactive cytosolic form (I), as shown in figure 1. Definitions and values of parameters are provided in appendix B, and table D1. We consider a 1D spatial domain where x is position along a 'cell diameter' and t is time. This model could describe a two-dimensional square cell, whose protein concentrations are constant in one direction [30]. Balance equations of the form

$$\frac{\partial A}{\partial t} = f + D_A \nabla^2 A, \tag{1a}$$

$$\frac{\partial I}{\partial t} = -f + D_I \nabla^2 I, \tag{1b}$$

along with no flux boundary conditions are used to describe the NPFs. The active form A is taken to be membrane bound whereas the inactive form, I, is cytosolic. Note that the total amount, $A + I$, is conserved by (1). We assume that A is slow diffusing and I is fast diffusing so that $D_A \ll D_I$. We use a simplified set of 'WP' kinetics [25]:

$$\text{wave-pinning:} \quad f = f(A, I) = \left(k_0 + \frac{\gamma A^n}{A_0^n + A^n}\right) I - \delta A, \tag{2}$$

motivated by previous work on GTPases [25], to describe cycling between active and inactive NPFs, figure 1. Briefly, k_0 is a basal activation rate and the Hill function represents autocatalytic positive feedback of A. The magnitude of that positive feedback is controlled by γ and the sharpness of the response is determined by the Hill coefficient n. A_0 is the typical level of A at which positive feedback 'turns on' and δ is the NPF inactivation rate. These terms are motivated biologically from known and hypothesized GTPase properties discussed in [34–36, 25].

Our model differs from those of others [7, 28, 29, 32] in several ways. In [7], the NPF is identified with Hem1, assumed to autoactivate from a fixed inactive pool. Iglesias *et al* [32] propose an excitable FitzHugh–Nagumo (FN) type wave generator with additional components to account for features such as persistence and polarity. A second model based on FN was proposed by [37] for the random appearance of transient patches of membrane-associated proteins typical of stimulated cellular slime mould (*Dictyostelium discoideum*) cells. There the patterns stem from noise in the local activation long-range inhibition that the authors assume. In [28], the NPFs also interconvert between active and inactive forms (with conserved total amount). Their kinetics are based on quadratic interaction terms (implying at most two steady states), whereas in our equation (2), the Hill function saturating positive feedback term means that up to three A steady states exist for fixed I. This distinction is an essential feature of our model that leads to a type of wave behaviour not present in [28]. Whitelam *et al* [29] take an altogether different approach and propose a model based on F-actin auto activation and degradation by another biochemical factor, not an NPF based model.

We embed these nucleation promoting factor kinetics in a circuit where the active NPF promotes F-actin (F) growth, which in turn feeds back to inhibit NPF activation, as shown in figure 1. F-actin plays the role of a refractory variable in the sense of excitable systems; that is, it locally suppresses NPF

activity to produce a quiescent spatial gap behind the NPF wave. F-actin is modelled by

$$\text{F-actin:} \quad \frac{\partial F}{\partial t} = \epsilon h, \tag{3a}$$

where h is a function of other variables (see below) and ϵ is a rate constant that represents the longer refractory timescale ($\tau = 1/\epsilon$) on which the actin kinetics occur relative to the NPF timescale. The NPF kinetics (1*a*), (1*b*) are modified to include negative feedback from F:

Modified NPF kinetics:

$$f(A, I, F) = \left(k_0 + \frac{\gamma A^3}{A_0^3 + A^3}\right) I - \delta\left(s_1 + s_2 \frac{F}{F_0 + F}\right) A. \tag{3b}$$

A Hill coefficient $n \geqslant 2$ is essential for WP behaviour. While $n = 2$ works, the relevant parameter regime for patterns is quite narrow, a problem that is corrected by using $n = 3$. The parameters s_1, s_2 represent the relative weighting of the basal versus the F-actin-mediated NPF inactivation rates. δ sets the overall timescale of NPF degradation. The pure NPF 'WP' scenario corresponds to $s_1 = 1$, $s_2 = 0$. Note that we do not include actin filament angular or length distributions.

It is assumed that the filamentous actin, F, is nucleated from a constant (non-depleting) pool of monomeric G-actin (G), whose level affects only the rate constant k_n. We thus take the function h to be

$$\text{F-actin kinetics:} \quad h(A, F) = k_n A - k_s F. \tag{4}$$

The combination ϵk_n is the rate of F-actin nucleation by NPF and ϵk_s is the F-actin disassembly rate. We assume that $D_A \ll D_I$ and that F is non-diffusive. Note that our calculations (not shown) indicate that taking F to be diffusive with $D_F \approx D_A$ does not appreciably affect the results. Substantially larger diffusion rates for F will however prevent waves from forming. Equations governing A, I, F are supplemented with no flux (homogeneous Neumann) boundary conditions and simulated numerically using the algorithm discussed in appendix D.

As we wish to focus on the role of feedback, we concentrate on the parameters s_1, s_2, k_0. The first two describe properties of feedback from actin to the NPFs, which is of primary interest here. The third (k_0), represents a basal NPF activation rate and is known to be a key parameter for determining the sensitivity of the NPF model to perturbations. We map the parameter space with respect to these parameters and outline the stability of spatially uniform steady state solutions to both small and large perturbations. In order to provide context, we compare properties of the model to two well-studied pattern forming systems: the FN model [38] and the WP model [25]. Aside from this discussion, further details are provided in the appendix.

Motivation for our models stems from the FN system (appendix A) where a bistable wave-generating component produces a moving front and a second refractory component suppresses the trailing edge to create a localized travelling wave or pulse (figure 2). The formation of that wave stems from the (cubic) reaction kinetics. Large amplitude limit cycles arise in the spatially-independent model leading to oscillation between high and low activity; diffusion simply causes these regions to propagate in space, as a localized travelling wave. (The limit cycle stems from a sub-critical Hopf bifurcation, i.e. oscillations appear suddenly with finite amplitude as a parameter is varied [39].) Our model builds on this general structure but with reaction kinetics that produce different stability properties and long term dynamics.

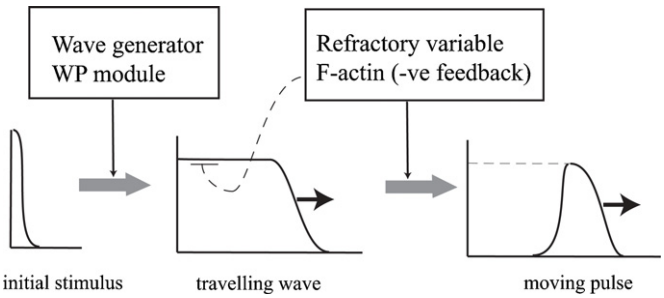

Figure 2. The FitzHugh–Nagumo model provides motivation for our representation of F-actin and NPF system. A wave-generator induces a travelling wave-front, which separates states of high and low NPF activity. The F-actin has the role of a refractory variable that suppresses the high trailing edge of the wave on a longer timescale, leading to a spatially localized wave.

In place of the bistable wave generator used in the FN model, our model uses the 'WP' model consisting of equations (1), (2) for the NPFs. As a stand alone model (i.e., no F feedback), it exhibits distinct regimes: (1) A classical 'Turing regime' where a uniform steady state is unstable to small spatially heterogeneous perturbations. (2) A 'WP regime' where the uniform steady state is stable to all small perturbations, but unstable to perturbations beyond some threshold amplitude. Such perturbations initiate a travelling wave of A that propagates into the domain, thereby depleting I, and causing the wave front to slow down and eventually stall in the domain interior (under appropriate conditions). This module serves as the wave initiator in our model.

3. Results

We now describe the behaviours predicted by our model, focusing on how patterns are generated and their long term dynamics. We discuss the effects of two model elements on pattern forming regimes: (1) conservation of the NPFs and (2) feedback between NPFs and F-actin. We show that the negative feedback produces oscillatory behaviour that sets up several types of localized travelling waves. These can arise either from an instability or from a distinct property, which we refer to as excitability, related to the WP regime in the NPF model. On long timescales, we find distinct wave propagation regimes that contrast with dynamics of the FN system and correspond to different cellular behaviours. We first describe these behaviours, determined using numerical simulations, then apply a nonlinear perturbation analysis to understand the structure of the parameter space that gives rise to them.

3.1. Spatiotemporal dynamics

We simulated our model for a range of parameter values. Here we describe the long time behaviour of patterns that result in

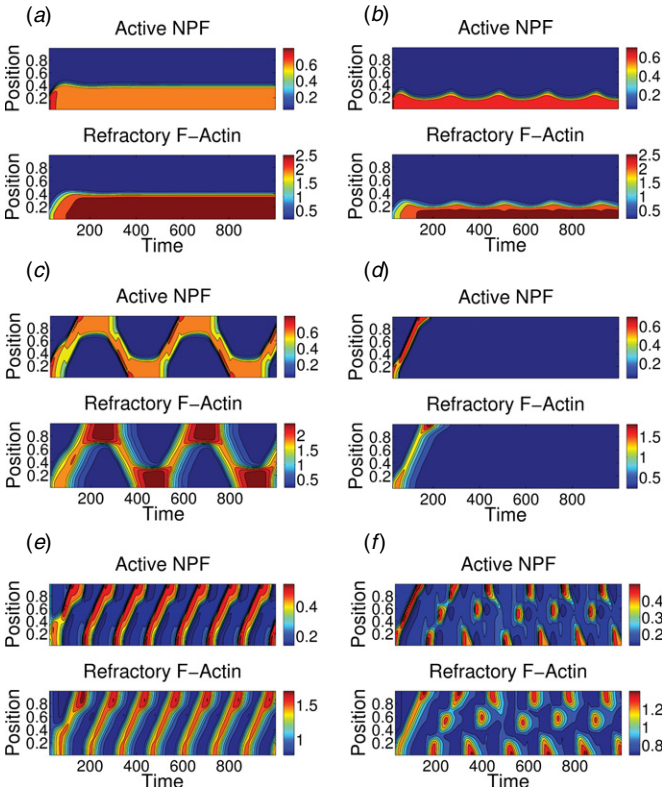

Figure 3. Simulations of our nucleation promoting factor/filamentous-actin (NFP/F-actin) model (equations (1), (3*b*), (3*a*), (4)) with a local perturbation at $x = 0$ used to initiate patterning. Parameter sets as in figure 5 and table D1. For example, panel (*a*) is simulated with the parameter set labelled '*a*' in figure 5. Panels (*a*)–(*d*) are computed at fixed k_0 with s_2 varied. As s_2 is increased, the behaviour undergoes a transition from stable boundary localized patterns (*a*), to oscillating boundary localized patterns (*b*), to reflecting waves (*c*), to a single terminating wave (*d*), to no patterning. Panels (*e*) show a wave train and panels (*f*) a more exotic pattern.

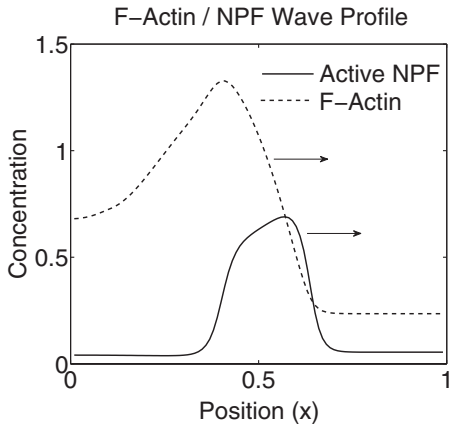

Figure 4. Snapshot of the localized travelling wave profile of F-actin, F, and NPF, A, from figure 3(*d*) at time $T = 95$. The wave of NPF leads, and is followed by a wave of F-actin. The F-actin suppresses the trailing edge of the NPF wave, producing a localized profile.

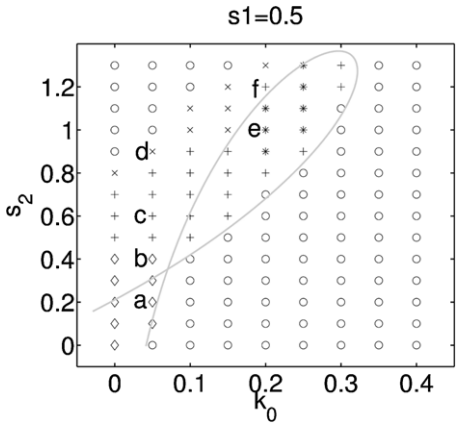

Figure 5. The k_0, s_2 parameter plane, showing regimes of distinct patterning for our nucleation promoting factor/filamentous-actin (NFP/F-actin) model (equations (1), (3*b*), (3*a*), (4)), as determined by full simulations of the full partial differential equation (PDE) model. Here, $s_1 = 0.5$, $\epsilon = 0.1$, and all other parameters as in table D1. Initial conditions: homogeneous steady state (HSS) with a region of elevated A level (local perturbation) superimposed at the boundary $x = 0$. Letters (a)–(f) correspond to patterns shown in the corresponding panels of figure 3. Symbols denote no patterning (o), boundary localized pattern (◊), persistent reflecting wave (+), single terminating wave (×), and persistent wave trains (∗). The grey curve is a two parameter continuation of the Hopf bifurcations in the local perturbation bifurcation plot of figure 6(*b*). The closed loop represents an approximate boundary of a region where an oscillatory instability exists for the full spatial RD system.

various parameter regimes. Representative results for $A(x, t)$ and $F(x, t)$ are shown in figure 3 as intensity plots in the (x, t) plane ('kymographs'). In each of these cases, patterning is induced with a localized perturbation of A at the $x = 0$ margin of the domain. While the dynamics for F and A are similar, the NPF pattern leads and the F-actin pattern lags behind in all cases. In figure 4 we show a typical set of profiles for the NPFs and F-actin corresponding to the behaviour shown in panel (*d*) of figure 3. The NPF is relatively localized, and leads at the front. The F-actin profile follows, with a broader trailing edge. Note that the width of the trailing edge is modulated by ϵ. We are primarily interested in exploring the influence of activation, inactivation, and feedback on dynamic behaviour. For this reason, we specifically focus on varying the parameters k_0, s_1, and s_2. Figure 5 depicts a representative (k_0, s_2) slice of the parameter space, subdivided into regimes based on long term evolution of patterns. Holding other parameters constant (table D1), we ran full PDE simulations for (k_0, s_2) grid values displayed in figure 5 and used an automated algorithm to classify the qualitative behaviour (appendix D). Labelled points correspond to the panels in figure 3, demonstrating simulation results in different regimes. The grey 'fish-shaped' bifurcation curve will be discussed in section 3.2.

Figure 5 and the associated kymographs in figure 3 show five primary patterning regimes (*a*)–(*e*) and several other exotic patterns that appear near borders between regimes, for example (*f*). Consider first the parameter sets in figure 3 (*a*)–(*d*). These are computed with a fixed value of k_0 and increasing values of s_2 to show the role of increasing F-actin feedback s_2. For low values of s_2, the local perturbation of activity at $x = 0$ leads to a pattern that localizes at the boundary and remains there. This is similar to the $s_2 = 0$ WP case. As s_2 is increased, we observe

a transition regime, in which the region of activity begins to oscillate near the boundary (*b*). It separates when the feedback strength is larger (*c*), and then a localized travelling wave traverses the domain. Upon reaching the opposite boundary, the active region resides there for a period of time before separating and crossing the domain again. We refer to this as 'reflecting wave' behaviour. At yet higher values of s_2 (*d*), once the wave arrives at the opposite boundary, it is suppressed. At even higher feedback strengths, regions of high activity never form. This progression shows that an appropriate level of feedback is essential: too little, and waves never propagate, too much and activity is simply suppressed.

Figure 3(*e*) shows a fifth type of behaviour. Here, a wave of activity traverses the domain and in its wake, the refractory F level falls low enough that a new wave of activity can form. This leads to a 'wave train'. Figure 5 shows that this behaviour exists at higher values of the basal NPF activation rate k_0 than for the reflecting waves. In this regime, if the domain size is increased, multiple waves coexist in time with a fixed separation distance determined by system parameters. Aside from the above five primary regimes, additional exotic patterns such as those shown in figure 3(*f*) are found in small regions at the boundaries of the primary regions. The full range of such exotic behaviour is beyond our scope here, and as these occur in limited parameter regions, our classification algorithm has not been designed to identify these details.

Figure 5 confirms that a balance between k_0 (NPF activation) and s_2 (F-actin mediated NPF inactivation) is required for patterning. The upper left corner (high F feedback and low NPF activation) and the bottom right corner (low F feedback and high NPF activation) both correspond to no patterning, with a region of dynamic patterning in between. Another feature of interest is the transient patterning band (indicated by the symbol $\times$) separating the upper left corner devoid of patterning and the band of persistent patterning. This shows that the transition between these regimes is not abrupt. In contrast, the transition to polarization type patterns at the bottom right corner is abrupt. The band of $\times$ represents transient single pulse of activity that traverses the domain. This type of pulse behaviour only occurs at large values of the feedback s_2. (At low values of s_2, polarized solutions are seen in place of pulse solutions so no such band of $\times$ is present at the lower boundary.) We constructed similar parameter planes for several values of s_1. These have similar structure, shifted due to increased basal inactivation for larger s_1.

3.2. Bifurcation analysis of a local approximation

We now use a bifurcation technique recently introduced by [40, 41] to map the parameter space of this model and detect the minimal stimuli needed to trigger patterning from a uniform state. For simplicity, the patterns in figure 3 are initiated with a (sufficiently large) perturbation of active NPF, A, at the boundary $x = 0$. However in some regimes, such a perturbation is not necessary and instability causes patterns to grow spontaneously from noise, even at very low level. Traditionally, linear stability analysis (LSA) is used to examine stability properties of a homogeneous (spatially uniform) steady state solution (HSS). Such analysis can reveal Turing-type instabilities, but cannot indicate whether larger amplitude perturbations grow or decay outside of these unstable regions. Furthermore, it becomes more challenging for models consisting of several variables, such as the one we propose.

Here we perform a nonlinear stability analysis of our model, exploiting the fast and slow diffusion scales to characterize the evolution of localized perturbations. This method, denoted 'local perturbation analysis' (LPA), and invented by Mareé and Grieneisen [40], uses a set of ordinary differential equations (ODEs) to approximate the partial differential equations (PDEs) by taking the limits $D_{\text{fast}} \to \infty$ and $D_{\text{slow}} \to 0$ where inactive NPF, I and active NPF and F-actin A, F are assumed to be fast and slow diffusing, respectively. The resulting system of ODEs (appendix C) describes the initial growth or decay of a localized perturbation (of arbitrarily small width) applied to the homogeneous steady state. An analysis of this system then provides an approximate bifurcation structure for the PDE system. This method is capable of detecting the presence of limit cycle oscillations (stemming from Hopf bifurcations in a well-mixed system) as well as spatial properties such as Turing instabilities, threshold responses such as wave-pinning [25], and other dynamics. While it is a powerful method for determining where patterning can occur and due to what mechanism, it does not predict long term dynamics. We thus connect this analysis to the full PDE simulations described above. Details of the approximating ODEs for the LPA are provided in appendix C with a more extensive description in [41, 42].

In figure 6, we show the LPA bifurcation plots for (*a*) the nucleation promoting factor (WP) model alone (equations (1)–(2)), and compare it to a similar plot in (*b*) for our NPF/F-actin model to contrast the differences and understand the effect of F-actin feedback. The bifurcation parameter is k_0, and the vertical axis is the amplitude of a localized perturbation of NPF activity (A^ℓ).

We first explain the interpretation of panel (*a*). The thick branch emanating from (0,0) and crossing the diagram represents the stability of the homogeneous steady state to simple noise (solid line for stable and dashed for unstable homogeneous steady state (HSS)). The thin looped branch represents stability of the HSS to the localized perturbation as follows. In region I, the HSS is stable with respect to small perturbations (both uniform and spatially nonuniform). The thin dashed line in this region indicates a threshold. A localized NPF perturbation whose magnitude is lower than this threshold level will decay back to the HSS. Once this threshold is breached, the perturbation will grow, jumping to the upper thin branch, a stable attractor. This indicates the initiation of a pattern. In region I, that pattern is the previously discussed 'WP' behaviour. This is the threshold-dependent (i.e., 'excitable') pattern-formation regime. As indicated by the bifurcation diagram, as k_0 increases in this region, the threshold that separates the homogeneous steady state from the patterned state diminishes. Once k_0 crosses the boundary of region II, a bifurcation occurs, indicated by the branch point where the thin and thick curves intersect. In that region, the HSS is unstable

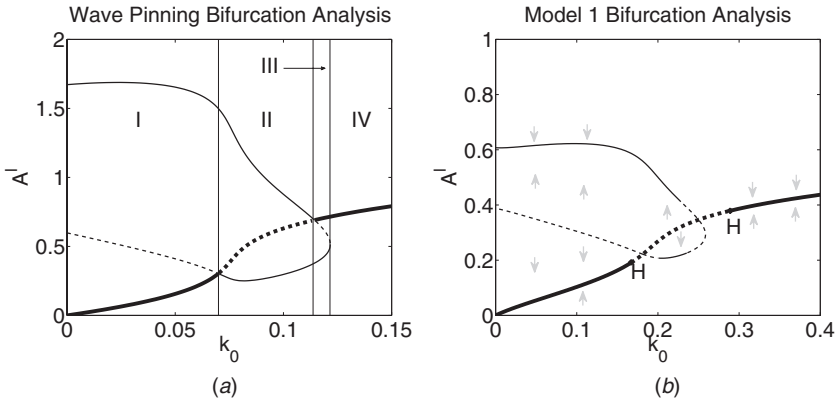

Figure 6. Nonlinear bifurcation analysis for (*a*) the wave-pinning model (equations (1), (2)), and (*b*) our NPF/F-actin model, (equations (1), (3*b*), (3*a*), (4)). Thick lines: HSS of the well-mixed system; thin lines: additional local states in the local perturbation system. Solid lines: stable states; dashed lines: unstable states. In (*a*), three patterning regions are observed: I, III—wave-pinning excitable response requiring a positive (respectively, negative) valued perturbation, II—unstable response. In region IV, the well mixed state is stable to all perturbations. Parameters used are $\gamma = K = \delta = 1$ with the conserved quantity $A + I = 2.27$, taken from [25]. In (*b*), the structure is similar to (*a*) but with two new Hopf bifurcations (H) resulting from F-actin feedback. Between these, there is an oscillatory instability leading to wave dynamics. Parameters: $s_1 = 0.7$, $s_2 = 0.7$, $\epsilon = 0.1$, and others as in table D1. Grey arrows indicate the stability of branches.

with respect to arbitrarily small spatial perturbations, as in classical Turing instability. In region III, the HSS is again stable to noise, but excitable by a sufficiently large negative valued local perturbation. In region IV, the HSS is stable to all perturbations, regardless of amplitude or sign. Thus, the results of LPA reveal two significant 'excitable' pattern forming regimes, I and III, and an unstable regime, II.

Comparing panels (*a*) and (*b*) of figure 6, we find the following common features. The shapes of the diagrams are similar, sharing branch point bifurcations separating regions that we recognize as excitable and unstable. We also find key differences. First, we see in panel (*b*) the appearance of a pair of Hopf bifurcations (labelled H). These new bifurcations indicate the presence of a regime of oscillatory behaviour (for a range of k_0 between the two H bifurcation values) that is not present in figure 6 (*a*) for the WP model on its own. This new feature stems directly from the F-actin negative feedback in our model for actin waves. We used a two-parameter continuation to follow the Hopf bifurcation points with respect to both k_0 and s_2. The result is shown as the grey curve superimposed on figure 5. Here, we are primarily concerned with the resulting loop that acts as an approximate boundary of a region where an oscillatory instability exists for the PDE system. While the loop is predicted by the approximate nonlinear bifurcation technique, it has good correspondence with a partition of parameter space into regions of instability (inside the loop) and excitability (outside).

To connect this stability discussion to the long-term behaviours described above, consider first the boundary-localized patterns of figure 3 (*a*), (*b*). These patterns appear only in the excitable region; the limit cycle oscillations that appear inside the loop are inconsistent with static spatial patterns. Similarly, the single wave solution of figure 3(*d*) occurs only in the excitable regime. This is not surprising since both patterns have a stable character that is inconsistent with an oscillatory instability. The wave train solution in figure 3(*e*), on the other hand, only occurs inside the unstable loop. The reflecting wave solution in figure 3(*c*) occurs in both regimes. Exotic patterns such as figure 3(*f*) appear near the edge of this loop. The consistency of the LPA results with the PDE simulation results confirms the relevance of the LPA to understanding long-term dynamic behaviour. As discussed in appendix C, the local perturbation approximation is, strictly speaking, valid only until the perturbation is no longer localized. In a separate article [42], asymptotic analysis is used to rigorously probe the comparison between this technique and more traditional asymptotics methods. However, as we have informally shown here, this nonlinear bifurcation method generally corresponds well to simulations of the full spatially explicit PDE model.

3.3. Insights from model studies

In summary of our nucleation promoting factor/F-actin model, intermediate levels of refractory feedback are required to induce dynamic patterning. Too little feedback leads to stable patterns akin to those seen in pure NPF (WP) model. As feedback is progressively increased, static patterns start to oscillate, then become travelling waves; further feedback kills the waves as they arrive at boundaries, and finally leads to loss of all patterning by strong damping of all perturbations. It was also found that in different regimes, the waves that result take the form of either wave trains or reflecting waves.

We point out a few substantive differences between the mathematical structure of our model and that of the FN model. The FN waves are driven by oscillations of the reaction kinetics and diffusion simply converts those oscillations to travelling waves. Thus, unstable regimes lead to persistent wave trains and excitable regimes lead to single travelling waves that leave the stable homogeneous steady state in their wake. The reaction kinetics in our NPF/F-actin model exhibit no such inherent oscillatory kinetics, and the resulting waves are, instead, driven by a combination of the wave-pinning structure in the NPF module, which is intimately tied to diffusion, and refractory feedback. This feature leads to distinct behaviours that are not observed in FN based models nor in other models based on a

Turing-type wave generator. (1) The model exhibits a transition between states of static polarization and states characterized by dynamic travelling wave patterns as the feedback strength is modulated. Such transitions could be induced experimentally if one could identify the binding domain that causes F-actin to pull NPFs off the membrane. Mutation of this domain would reduce the negative feedback and thus cause a transition from oscillating waves to static polarization. (2) Regimes exist where a transient stimulus will excite a stable homogeneous state, inducing persistent travelling wave dynamics. Such a stimulus could be achieved by transient photoactivation of Rho GTPases [43]. (3) Within the regime of persistent patterns shown in figure 5 there is a wealth of dynamics that includes reflecting waves, wave trains, and boundary localization.

4. Conclusions

As shown in this paper, a small extension of a minimal model for Rho-GTPase (wave-pinning) dynamics [25] to include feedback from F-actin leads to a variety of novel spatiotemporal dynamics. The general structure of our nucleation promoting factor (NPF)/F-actin model was motivated by two systems, the FitzHugh–Nagumo (FN) model for impulse propagation in neurons and the 'wave-pinning' model for small GTPases in eukaryotic cells, chosen here to represent a NPF. It was shown that the NPF triggers initial pattern formation and refractory F-actin produces spatially localized travelling waves. The resulting model exhibits a rich collection of dynamics including static polarization and boundary localized patterns, single waves, reflecting waves, wave trains and more exotic patterns. The identification of NPFs with small GTPases is one hypothesis that distinguishes our model from other current models. This idea is based on extensive evidence for actin assembly downstream of Cdc42, Rac, and Rho [2, 3, 44], and on experimental observations that actin feedback affects PI3K-mediated pathways [16, 18, 19], and integrin signalling [21, 22] that are, in turn, known to affect small GTPases. However, many of our results would hold equally well for interpretations of A, I as forms of other actin-promoting factors with membrane bound and free cytosolic forms that interconvert rapidly.

To gain a better understanding of the parameter space and modes of pattern formation, we analysed these systems with a relatively new nonlinear stability analysis that considers stability of homogeneous steady states with respect to localized perturbations. This analysis revealed the presence of two stability regimes, 'excitable' and unstable with the transition between them occuring at a PDE-variant of a Hopf bifurcation. In the first, only perturbations whose magnitude exceeds a threshold can trigger a pattern, whereas in the second, patterns arise from arbitrarily small noise. Combining these results with simulations, we connected the long term behaviour of patterns to these stability regimes. We found that wave trains are instability driven, reflecting waves occur in both regimes, and both transient wave and boundary localized patterns are present in excitable regimes. We subsequently suggested observed actin patterning phenomena to which these behaviours relate.

These systems are distinct from other current 'actin waves' models [7, 28, 29, 32] both in structure and in richness of behaviours. The models in [7, 28] are designed around NPF models with unstable homogeneous steady states and do not exhibit excitable behaviour. The model in Whitelam *et al* [29] is structurally distinct, hypothesizing that a biochemical inhibitor is responsible for patterning as opposed to an NPF. Being a direct extension of the FN model, it also likely does not account for persistent patterning outside of unstable regimes, a key requirement for stable systems that show persistent responses to transient stimuli. Yet another model for actin waves by [45] is based on an entirely different mechanism of membrane curvature. See also alternative models proposed by [46, 47]. Our model thus suggests a mechanism for actin patterning that is substantially different from previous work on the topic and exhibits a broader range of behaviours.

While our model is simplified for maximal insight (and therefore not a detailed description of cellular events), it is tempting to draw connections between the dynamics predicted by our model and phenomena that are observed experimentally. The static boundary-localized pattern observed in figure 3(*a*) is indicative of a static polarization associated with chemotaxis, where the NPF and F-actin co-localize at the front of a lamellipodium.

The oscillating boundary pattern in figure 3(*b*) is reminiscent of experiments in which the leading edge of the lamellipodium oscillates [48]. The NPF in the simulations remains at one end of the cell, but its accumulation oscillates. This leads to oscillating actin polymerization, which would exert an oscillatory force on the membrane, causing cyclic protrusion. Several types of oscillating membrane morphologies were observed in [48]. Their 'I' state displayed oscillations perpendicular to the membrane, with a fairly constant profile parallel to the membrane. We believe that our oscillations may be related to these. The 'I' state was induced by constitutive activation of the Rho GTPase Rac1, supporting the assumption that Rho GTPases are relevant to the dynamic behaviours found here. The travelling wave patterns in figures 3 (*c*)–(*e*) are similar to actin wave patterns observed in [5, 6], with clearest data in [7, 8, 10]. Gerisch *et al* [10] showed several examples of waves reflecting from the boundary, as in figure 3(*c*). Weiner *et al* [7] and Millius *et al* [8] showed single pulses or trains of pulses extinguishing at the boundary, as in figures 3(*d*) and (*e*), or persisting at the boundary as in 3(*a*).

Developing a broad based conceptual framework for interpreting experimental observations and transitions between different dynamical behaviours has been a key goal of this work. Our model is a minimal representation of actin-NPF dynamics. In one sense, it is simpler than other current models, as we made no attempt to represent actin filament length or orientation that others consider [28, 29, 30, 31]. The absence of these details here indicates that, at least from the perspective of pattern dynamics and richness, the model structure is as important as biophysical details of F-actin. From a biophysical perspective, it is important to determine whether or not the feedbacks proposed here occur and are relevant to the formation of dynamic actin structures, and if so, what factors mediate that feedback. From a theoretical perspective, it is important to gain a more complete understanding of the

propagation of these patterns and their connection to stability regimes.

Acknowledgments

This work was supported by the National Institutes of Health under grant R01 GM086882 (to AEC and LEK) and an NSERC discovery grant (to LEK).

Appendix A. The FitzHugh–Nagumo model

The FitzHugh–Nagumo (FN) model [38], depicted in figure 2 is given by the equations

$$\frac{\partial v}{\partial t} = f(v) - w + \gamma + \nabla^2 v, \qquad \frac{\partial w}{\partial t} = a(bv - cw) \tag{A.1a}$$

where f is the cubic

$$f(v) = dv(v-1)(\alpha - v). \tag{A.1b}$$

Originally meant as a caricature of impulse propagation in axons, v is identified with a fast-changing membrane voltage and w represents a more slowly varying property of ion channels. For sufficiently large γ, a wave of v propagates, increasing w in its wake. On a slightly longer timescale, increased w causes v to decrease leading to an impulse.

In this system, wave formation is driven almost exclusively by the reaction kinetics independent of any diffusive effects. A sub-critical Hopf bifurcation arises as γ is varied, leading to large amplitude limit cycle oscillations where v oscillates between two stable branches of the bistable kinetics for v. Further, the FN system demonstrates two behaviours. (1) Instability of the homogeneous steady state (HSS) gives rise to persistent oscillations in the reaction kinetics and persistent wave behaviour in the PDEs. (2) The HSS is stable and a large perturbation can give rise to a single wave which decays back to that state.

We point out these properties to contrast them with those of our model. The wave generating NPF reaction kinetics for our model do not exhibit limit cycle oscillations. Our wave generating NPF variable A, which is akin to v, is monostable. Instead, a distinct 'wave-pinning' property that we describe next gives rise to waves. This distinction leads to the behaviours discussed in the main text.

Appendix B. Wave pinning

The NPF module was motivated by the 'wave-pinning' (WP) model for polarization of small GTPases [34–36, 25, 49], proposed as a mechanism for breaking symmetry and generating polarized patterns in cells. The WP model (figure 1(*a*)) is described by equations (1), (2). Under the assumption $D_A \ll D_I$, this model exhibits two basic pattern forming regimes shown in figure 6(*a*): a classical Turing regime (region II) and a WP regime (regions I, III). In the Turing regime, a single steady state of the well mixed kinetics is linearly stable in a well mixed sense but unstable to heterogeneous noise. In the wave-pinning regime, a single steady state exists and is both linearly and turing stable. Thus, the well mixed kinetics alone do not suggest any pattern forming behaviour as is the case in the FN model. In this regime however, sufficiently large perturbations (indicated by the separation between thick and thin lines in figure 6(*a*)) can initiate a travelling wave of high activity. As this wave propagates into the domain, it depletes the background inactive form I causing the wave to slow down, and in appropriate parameter regions, stall in the interior. Where bistability serves to initiate waves in the FN model, this mechanism serves as the primary wave generating component in our model. See [25, 27] for further exposition of wave-pinning.

Appendix C. Nonlinear bifurcation analysis

The bifurcation analysis discussed in this paper is based on a nonlinear analysis that determines the stability of a homogeneous steady state (HSS) with respect to localized perturbations. The method, called the 'local perturbation analysis' (LPA) was first introduced in [40] and more extensively developed in [41, 42]. We briefly describe it here. Consider a system of reaction diffusion (RD) equations with slow diffusing (u) and fast diffusing (v) variables

$$\frac{\partial u}{\partial t}(x,t) = f(u,v) + D_u \nabla^2 u, \tag{C.1}$$

$$\frac{\partial v}{\partial t}(x,t) = g(u,v) + D_v \nabla^2 v. \tag{C.2}$$

Here $D_v \gg D_u$ and $x \in R^d$. (We identify u with active NPF, A, and actin F; v represents the fast diffusing inactive NPF, I.) For simplicity, in this exposition we consider one slow and one fast diffusing variable. However, the method can be extended to consider families of slow (respectively fast) variables so that u, v are vectors.

Consider the limit $D_v \to \infty$. In this limit, the fast variable has only a global, homogeneous behaviour due to the very large diffusive length scale. Further, take the limit $D_u \to 0$ so that the slow variable has a purely local behaviour. Now apply a local perturbation to the slow variable u (figure C1). Then to a good approximation, u has a purely local behaviour (u_l) near the perturbation, and a uniform global level (u_g) elsewhere, which do not interact through diffusion when $D_u \to 0$. Here u_l represents the amplitude of the narrow perturbing pulse, and u_g the background level of u that has been perturbed. In contrast, v is purely global (v_g) since in the limit $D_v \to \infty$, spatial inhomogeneities are smoothed out immediately. Hence, $v_g \approx v$ is the background level of v. The system of RD equations (C.1) can now be approximated by a set of ODEs

$$\begin{aligned} \frac{\mathrm{d}u_g}{\mathrm{d}t}(x,t) &= f(u_g, v_g), \\ \frac{\mathrm{d}v_g}{\mathrm{d}t}(x,t) &= g(u_g, v_g), \\ \frac{\mathrm{d}u_l}{\mathrm{d}t}(x,t) &= f(u_l, v_g). \end{aligned} \tag{C.3}$$

This approximation holds for some time until the perturbation is no longer localized.

Ordinary differential equations have an advantage that automated bifurcation techniques can be applied, using one

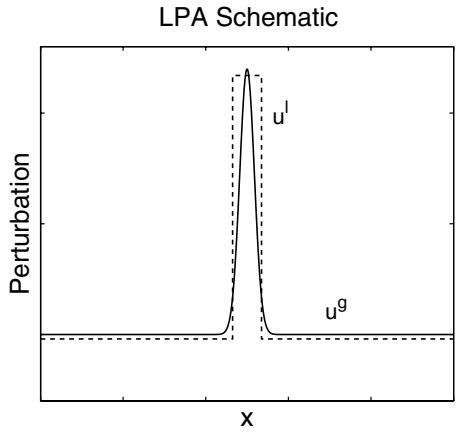

Figure C1. Schematic diagram of the local perturbation of u on which the 'local perturbation analysis' (LPA) approximation is based. In the limit $D_u \ll D_v$, u takes on a local behaviour near the perturbation and another, global, behaviour elsewhere. Here u^l, the amplitude of the narrow perturbing pulse is the 'local variable', u^g, the background level of u is the 'global' u variable. The fast diffusing variable v (not depicted) takes on a uniform global level, $v \approx v^g$ as any inhomogeneities are quickly smoothed out. The dashed line depicts the idealized local perturbation in the LPA diffusion limit, and the solid line is its realistic counterpart, where small but finite diffusion of u causes a slight outwards spread.

of several available software packages. (Partial differential equations are still largely managed on a case-by-case basis.) As described in the main text, the bifurcation analysis of this reduced approximation provides information about the initial growth or decay of a localized perturbation in the RD system. A primary benefit of this method is that the applied local perturbation is of arbitrary height whereas other stability methods only consider small perturbations and cannot detect threshold behaviour. When the diffusion disparity in (C.1) is moderately large, the approximation leads to predictions about parameter dependence and types of pattern-forming instabilities that closely match the simulated behaviour of the full RD system. The local pulse analysis is valid for a timescale that is shorter than the slow diffusion timescale (over which perturbations spread). For example, taking a pulse-spreading length scale on the order of 10% of the domain, the slow diffusion timescale would be $(0.1L)^2/D_A \approx 30$ (see table D1), a rough outer limit for the validity of LPA. The approximation does not provide direct information about long term dynamics of the pattern; for this reason, full simulations of the PDEs are still needed. We emphasize that all results were checked with full simulation and that LPA was used only as a guide. However, having this tool to map out relevant parameter regimes, and to see how changes in the structure of the model affect its overall behaviour proves enormously useful.

We demonstrate this analysis for the WP system in appendix B. We identify A and I as the slow and fast diffusing quantities in equations 1. The reduced system of ODEs describing the stability of this system to local perturbations are

$$\frac{dA_g}{dt} = \left(k_0 + \frac{\gamma A_g^n}{k^n + A_g^n}\right) I_g - \delta A_g, \tag{C.4}$$

$$\frac{dI_g}{dt} = -\left(k_0 + \frac{\gamma A_g^n}{k^n + A_g^n}\right) I_g + \delta A_g, \tag{C.5}$$

$$\frac{dA_l}{dt} = \left(k_0 + \frac{\gamma A_l^n}{k^n + A_l^n}\right) I_g - \delta A_l. \tag{C.6}$$

As before, here A_l is the amplitude of the thin localized perturbing pulse of A, whereas A_g the background global level of A that has been perturbed. Similarly, $I \approx I_g$ is the background global level of the inactive NPF. Conservation of these forms under the assumption that A_l is confined to a local spatial region implies that $A_g + I_g = T$ where T is the total conserved amount of material. The system then reduces to

$$\frac{dA_g}{dt} = \left(k_0 + \frac{\gamma A_g^n}{k^n + A_g^n}\right)(T - A_g) - \delta A_g, \tag{C.7}$$

$$\frac{dA_l}{dt} = \left(k_0 + \frac{\gamma A_l^n}{k^n + A_l^n}\right)(T - A_g) - \delta A_l. \tag{C.8}$$

A bifurcation analysis of this system using k_0 as the bifurcation parameter produces figure 6(*a*). The thick branch of states represents the HSS where no inhomogeneity is present ($A_l = A_g$). The thin branches represent patterned states where $A_g \neq A_l$.

Appendix D. Simulation methods

All numerical simulations of the full system of RD equations were carried out with an implicit-diffusion explicit-reaction numerical scheme coded in MatLab (MathWorks). In all cases homogeneous Neumann boundary conditions were applied and 100 grid points were used. In figures 3, 5, a pulse of A was applied to 5% of the spatial domain closest to the boundary $x = 0$ to induce patterning, but a similar pulse in any other location would suffice. Similarly, perturbations in the form of a gradient also induce pattern but with different response thresholds. Bifurcation diagrams were produced using MatCont [50], a numerical continuation package designed in MatLab.

An automated algorithm was developed in MatLab to analyse the spatio-temporal pattern resulting from the full RD simulations. Spatial profiles were computed and stored at time intervals $\Delta T = 5$ for each simulation. At each of these times, the maximum ('max') and minimum ('min') values of A over space were determined, as well as their spatial locations. From this, the velocity of the maximum point was computed. This information was used to classify the solution type using the following three criteria.

(1) If $|\max(A) - \min(A)| < \eta = 0.05$ for all $T > 500$, the pattern is classified as transient. Otherwise it is called persistent.
(2) If the location of the maximum is biased toward one domain boundary for all $T > 500$, the pattern is classified as boundary localized. Otherwise it is classified as dynamic.
(3) If the maximum point moves in the same direction (i.e. its velocity has a fixed sign) for more than 2/3 of the time, the wave is classified as unidirectional. Otherwise it is classified as reflecting.

Table D1. Parameters used for our model. Typical units would be μM (concentration), μm (distance) and s (time). NPF parameters are modified from [25] and actin parameters are chosen to illustrate a range of interesting dynamical behaviours.

Parameter name	Value	Units
k_0	0–1	Time^{-1}
γ	1	Time^{-1}
A_0	0.4	(concentration)
δ	1	Time^{-1}
s_1	0–2	Unitless
s_2	0–2	Unitless
F_0	0.5	(concentration)
k_n	1	Unitless
k_s	0.25	Unitless
T_{NPF}	1	(concentration)$\times$length
ϵ	0.1	Time^{-1}
L	1	Length
D_A, D_I	$10^{-3}/3$, $10^{-1}/3$	Length^2 Time^{-1}

These criteria can be used to classify the following pattern formation regimes demonstrated in figure 3: no pattern (not shown), boundary localized pattern as in panels (*a*), (*b*), persistent reflecting wave (*c*), single terminating wave (*d*), wave train (*e*). More exotic patterns such as figure 3(*f*) that were not the focus of this investigation can be misclassified by this algorithm.

References

[1] Mackay D J G and Hall A 1998 Rho GTPases *J. Biol. Chem.* **273** 20685–8

[2] Ridley A J 2006 Rho GTPases and actin dynamics in membrane protrusions and vesicle trafficking *Trends Cell Biol.* **16** 522–9

[3] Hall A 1998 Rho GTPases and the actin cytoskeleton *Science* **279** 509–14

[4] Sit S-T and Manser E 2011 Rho GTPases and their role in organizing the actin cytoskeleton *J. Cell Sci.* **124** 679–83

[5] Vicker M G 2002 F-actin assembly in *Dictyostelium* cell locomotion and shape oscillations propagates as a self-organized reaction-diffusion wave *FEBS Lett.* **510** 5–9

[6] Vicker M G 2002 Eukaryotic cell locomoation depends on the propagation of self-organized reaction-diffusion waves and oscillations of actin filament assembly *J. Expt. Cell Res.* **275** 54–66

[7] Weiner O D, Marganski W A, Wu L F, Altschuler S J and Kirschner M W 2007 An actin-based wave generator organizes cell motility *PLoS Biol.* **5** 2053–63

[8] Millius A, Dandekar S N, Houk A R and Weiner O D 2009 Neutrophils establish rapid and robust wave complex polarity in an actin-dependent fashion *Curr. Biol.* **19** 253–9

[9] Bretschneider T, Diez S, Anderson K, Heuser J, Clarke M, Mueller-Taubenberger A, Koehler J and Gerisch G 2004 Dynamic actin patterns and arp2/3 assembly at the substrate-attached surface of motile cells *Curr. Biol.* **14** 1–10

[10] Gerisch G, Bretschneider T, Müller-Taubenberger A, Simmeth E, Ecke M, Diez S and Anderson K 2004 Mobile actin clusters and traveling waves in cells recovering from actin depolymerization *Biophys. J.* **87** 3493–503

[11] Bretschneider T, Anderson K, Ecke M, Müller-Taubenberger A, Schroth-Diez B, Ishikawa-Ankerhold H C and Gerisch G 2009 The three-dimensional dynamics of actin waves, a model of cytoskeletal self-organization *Biophys. J.* **96** 2888–900

[12] Xiong Y, Huang C-H, Iglesias P A and Devreotes P N 2010 Cells navigate with a local-excitation, global-inhibition-biased excitable network *Proc. Natl. Acad. Sci.* **107** 17079–86

[13] Schroth-Diez B, Gerwig S, Ecke M, Hegerl R, Diez S and Gerisch G 2009 Propagating waves separate two states of actin organization in living cells *HFSP J.* **3** 412–27

[14] Gerisch G 2010 Self-organizing waves that simulate phagocytic cup structures *PMC Biophys.* **3** 7

[15] Driscoll M K, McCann C, Kopace R, Homan T, Fourkas J T, Parent C and Losert W 2012 Cell shape dynamics: from waves to migration *PLoS Comput. Biol.* **8** e1002392

[16] Xu J, Wang F, Keymeulen A Van, Herzmark P, Straight A, Kelly K, Takuwa Y, Sugimoto N, Mitchison T and Bourne H R 2003 Divergent signals and cytoskeletal assemblies regulate self-organizing polarity in neutrophils *Cell* **114** 201–14

[17] Sasaki A T, Chun C, Takeda K and Firtel R A 2004 Localized Ras signaling at the leading edge regulates PI3K, cell polarity, and directional cell movement *J. Cell Biol.* **167** 505–18

[18] Sasaki A T, Janetopoulos C, Lee S, Charest P G, Takeda K, Sundheimer L W, Meili R, Devreotes P N and Firtel R A 2007 G protein–independent Ras/PI3K/F-actin circuit regulates basic cell motility *J. Cell Biol.* **178** 185–91

[19] Weiner O D, Neilsen P O, Prestwich G D, Kirschner M W, Cantley L C and and H R Bourne 2002 A PtdInsP3-and Rho GTPase-mediated positive feedback loop regulates neutrophil polarity *Nature Cell Biol.* **4** 509–13

[20] Wang F, Herzmark P, Weiner O D, Srinivasan S, Servant G and H R Bourne *et al* 2002 Lipid products of pi (3) ks maintain persistent cell polarity and directed motility in neutrophils *Nature Cell Biol.* **4** 513–8

[21] Calderwood D A, Shattil S J and Ginsberg M H *et al* 2000 Integrins and actin filaments: reciprocal regulation of cell adhesion and signaling *J. Biol. Chem.* **275** 22607–10

[22] Abram C L and Lowell C A 2009 The ins and outs of leukocyte integrin signaling *Annu. Rev. Immunol.* **27** 339

[23] Otsuji M, Ishihara S, Carl C, Kaibuchi K, Mochizuki A and Kuroda S 2007 A mass conserved reaction–diffusion system captures properties of cell polarity *PLoS Comput. Biol.* **3** e108

[24] Goryachev A B and Pokhilko A V 2008 Dynamics of Cdc42 network embodies a turing-type mechanism of yeast cell polarity *FEBS Lett.* **582** 1437–43

[25] Mori Y, Jilkine A and Edelstein-Keshet L 2008 Wave-pinning and cell polarity from a bistable reaction-diffusion system *Biophys. J.* **94** 3684–97

[26] Jilkine A and Edelstein-Keshet L 2011 A comparison of mathematical models for polarization of single eukaryotic cells in response to guided cues *PLoS Comput. Biol.* **7** e1001121

[27] Mori Y, Jilkine A and Edelstein-Keshet L 2011 Asymptotic and bifurcation analysis of wave-pinning in a reaction-diffusion model for cell polarization *SIAM J. Appl. Math.* **71** 1401–27

[28] Doubrovinski K and Kruse K 2008 Cytoskeletal waves in the absence of molecular motors *Europhys. Lett.* **83** 18003

[29] Whitelam S, Bretschneider T and Burroughs N J 2009 Transformation from spots to waves in a model of actin pattern formation *Phys. Rev. Lett.* **102** 198103

[30] Carlsson A E 2010 Dendritic actin filament nucleation causes traveling waves and patches *Phys. Rev. Lett.* **104** 228102

[31] Doubrovinski K and Kruse K 2011 Cell motility resulting from spontaneous polymerization waves *Phys. Rev. Lett.* **107** 258103

[32] Iglesias P A and Devreotes P N 2012 Biased excitable networks: how cells direct motion in response to gradients *Curr. Opin. Cell Biol.* **24** 245–53
[33] Carlsson A E 2010 Actin dynamics: from nanoscale to microscale *Annu. Rev. Biophys.* **39** 91–110
[34] Maree A F M, Jilkine A, Dawes A, Grieneisen V A and Edelstein-Keshet L 2006 Polarization and movement of keratocytes: A multiscale modelling approach *Bull. Math. Biol.* **68** 1169–211
[35] Jilkine A, Maree A F M and Edelstein-Keshet L 2007 Mathematical model for spatial segregation of the Rho-Family GTPases based on inhibitory crosstalk *Bull. Math. Biol.* **69** 1943–78
[36] Dawes A T and Edelstein-Keshet L 2007 Phosphoinositides and rho proteins spatially regulate actin polymerization to initiate and maintain directed movement in a one-dimensional model of a motile cell *Biophys. J.* **92** 744–68
[37] Hecht I, Kessler D A and Levine H 2010 Transient localized patterns in noise-driven reaction-diffusion systems *Phys. Rev. Lett.* **104** 158301
[38] FitzHugh R 1969 *Mathematical Models of Excitation and Propagation in Nerve* vol 1 (New York: McGraw-Hill) pp 1–85
[39] Strogatz S H 1994 *Nonlinear Dynamics and Chaos: With Applications to Physics, Biology, Chemistry, and Engineering* (Cambridge, MA: Westview)
[40] Grieneisen Veronica 2009 Dynamics of auxin patterning in plant morphogenesis *PhD Thesis* University of Utrecht
[41] Holmes W R, Edelstein-Keshet L, Marée S and Gieneisen V 2012 The local perturbation analysis: a method for detecting spatio-temporal pattern forming capabilities in fast-slow reaction diffusion systems in preparation
[42] Holmes W R 2012 A local nonlinear stability analysis for reaction diffusion systems *SIAM J. Appl. Math.* submitted arXiv:1206.1985
[43] Wu Y I, Frey D, Lungu O I, Jaehrig A, Schlichting I, Kuhlman B and Hahn K M 2009 A genetically encoded photoactivatable rac controls the motility of living cells *Nature* **461** 104–8
[44] Pollard T D and Borisy G G 2003 Cellular motility driven by assembly and disassembly of actin filaments *Cell* **112** 453–65
[45] Peleg B, Disanza A, Scita G and Gov N 2011 Propagating cell-membrane waves driven by curved activators of actin polymerization *PLoS One* **6** e18635
[46] Ryan G L, Petroccia H M, Watanabe N and Vavylonis D 2012 Excitable actin dynamics in lamellipodial protrusion and retraction *Biophys. J.* **102** 1493–502
[47] Enculescu M, Sabouri-Ghomi M, Danuser G and Falcke M 2010 Modeling of protrusion phenotypes driven by the actin-membrane interaction *Biophys. J.* **98** 1571–81
[48] Machacek M and Danuser G 2006 Morphodynamic profiling of protrusion phenotypes *Biophys. J.* **90** 1439–52
[49] Goehring N W, Trong P K, Bois J S, Chowdhury D, Nicola E M, Hyman A A and Grill S W 2011 Polarization of PAR proteins by advective triggering of a pattern-forming system *Science* **334** 1137–41
[50] Dhooge A, Govaerts W and Kuznetsov Yu A 2003 MATCONT: A MATLAB package for numerical bifurcation analysis of ODEs *ACM Trans. Math. Softw.* **29** 141–64